Supplement of Atmos. Chem. Phys., 23, 12477–12503, 2023
https://doi.org/10.5194/acp-23-12477-2023-supplement

Atmospheric Chemistry and Physics
Open Access
EGU

Supplement of

Using synthetic case studies to explore the spread and calibration of ensemble atmospheric dispersion forecasts

Andrew R. Jones et al.

Correspondence to: Andrew R. Jones (andrew.jones@metoffice.gov.uk)

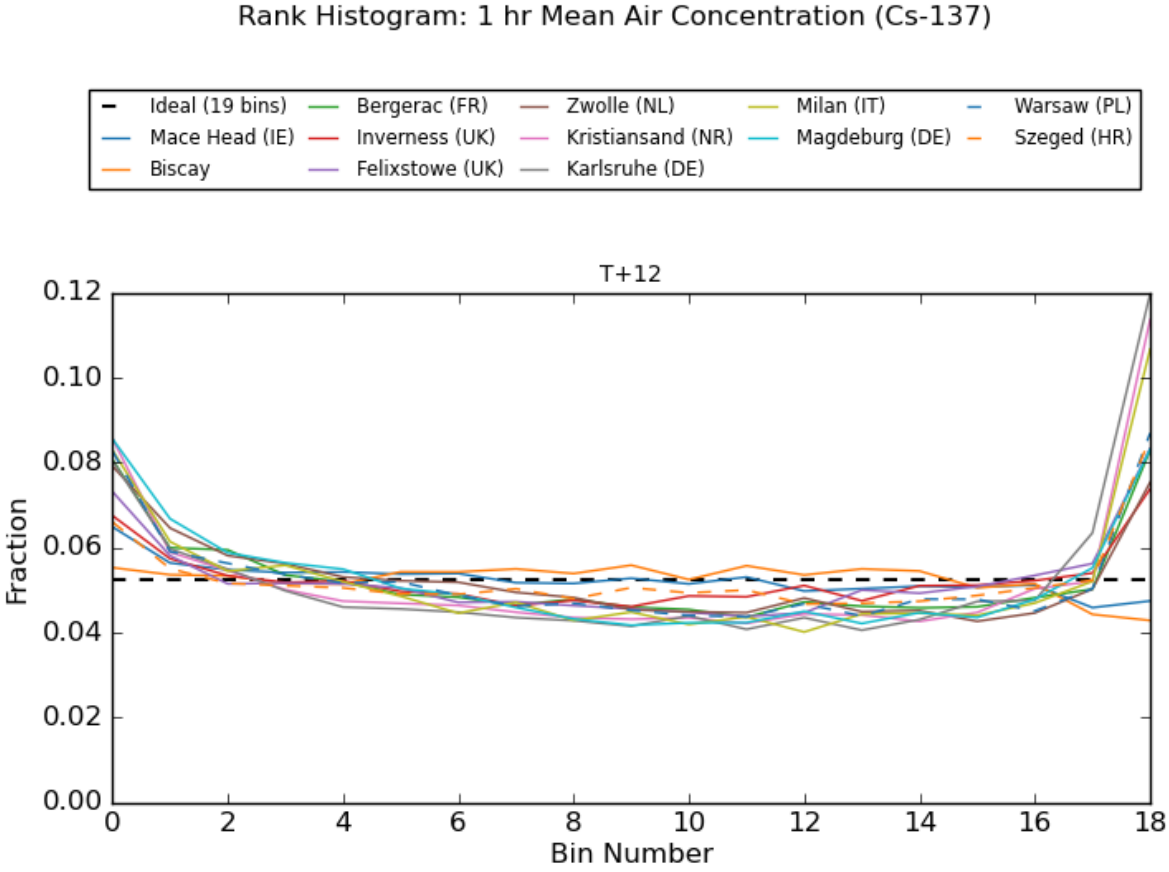

Figure S1. Rank histograms for 1-hour averaged air concentration after 12 hours from the start of the release. Data are shown for the 12 release locations separately.

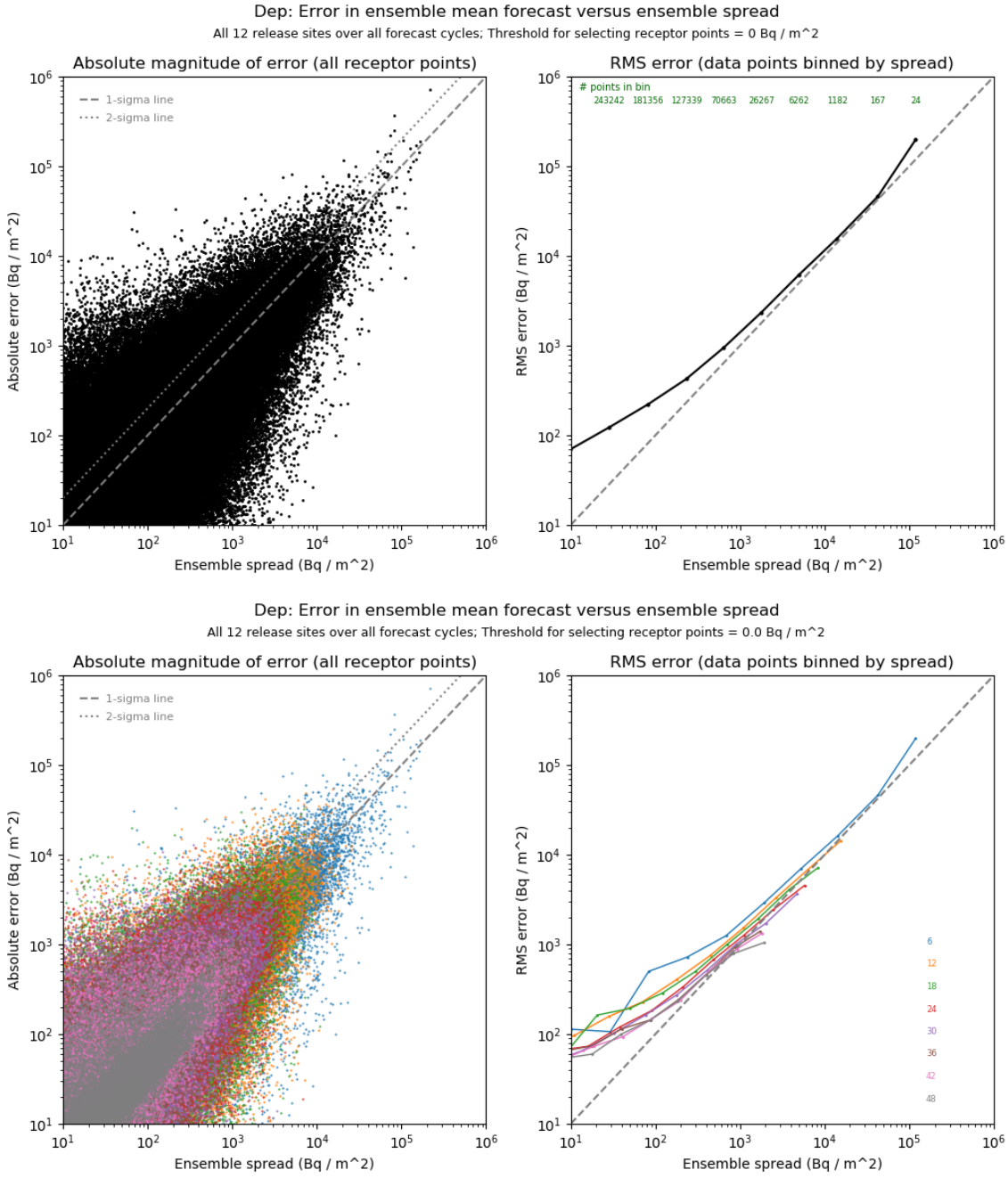

Figure S2. Comparison of ensemble spread against error in the ensemble mean forecast for 1-hour deposition at 6 hour intervals from the start of the release. In the upper plots, all time steps are combined, whereas lower plots show the split by time step. Note the log scaling used in each plot, and the overall decrease in magnitudes as the time step increases due to progressive dilution of plumes. Plots are based on combined data for all 12 release locations.

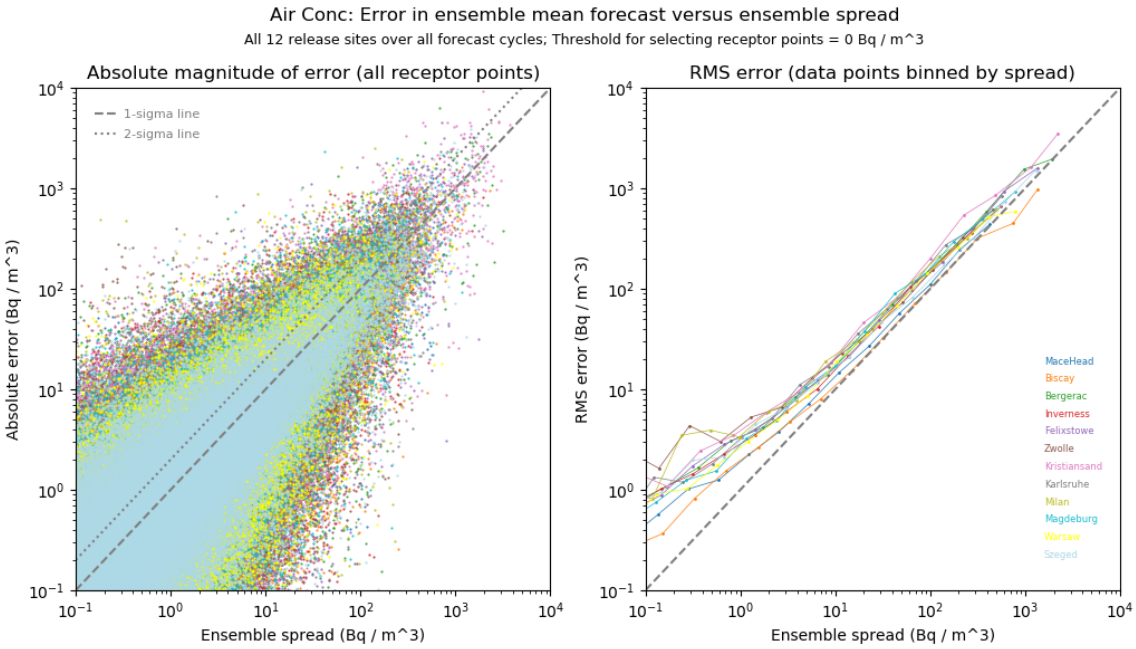

Figure S3. Comparison of ensemble spread against error in the ensemble mean forecast for 1-hour averaged air concentration at 6 hour intervals, comparing the releases from each location.

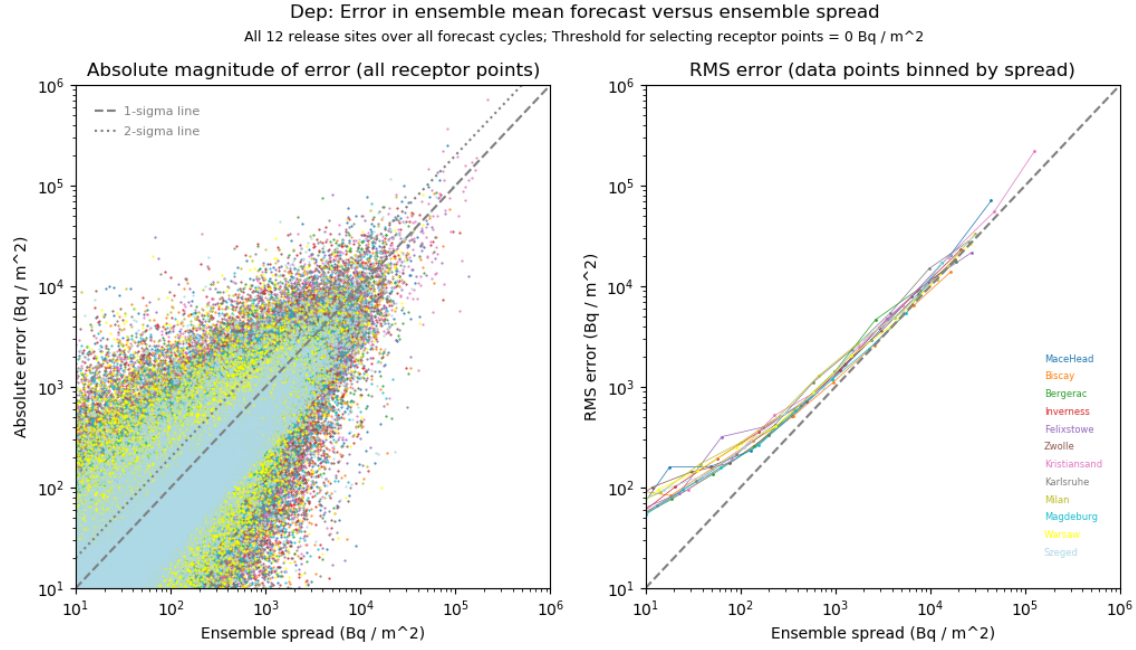

Figure S4. Comparison of ensemble spread against error in the ensemble mean forecast for 1-hour deposition at 6 hour intervals, comparing the releases from each location.

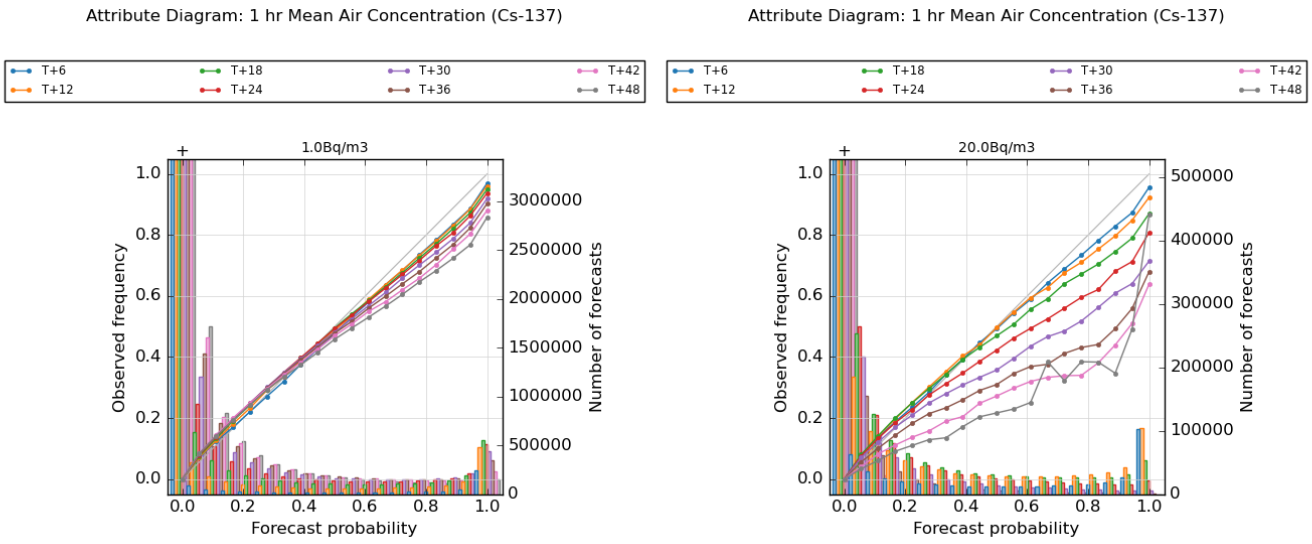

Figure S5. Attribute diagrams for threshold exceedances of 1.0 Bq m^{-3} (left) and 20.0 Bq m^{-3} (right) for the 1-hour averaged air concentration at 6 hour intervals through the forecast period. Plots are based on combined data for all 12 release locations. Note that the calibration function is beginning to become noisy towards the end of the simulation for the 20.0 Bq m^{-3} threshold due to the fall off in the number of sample points reaching this threshold.

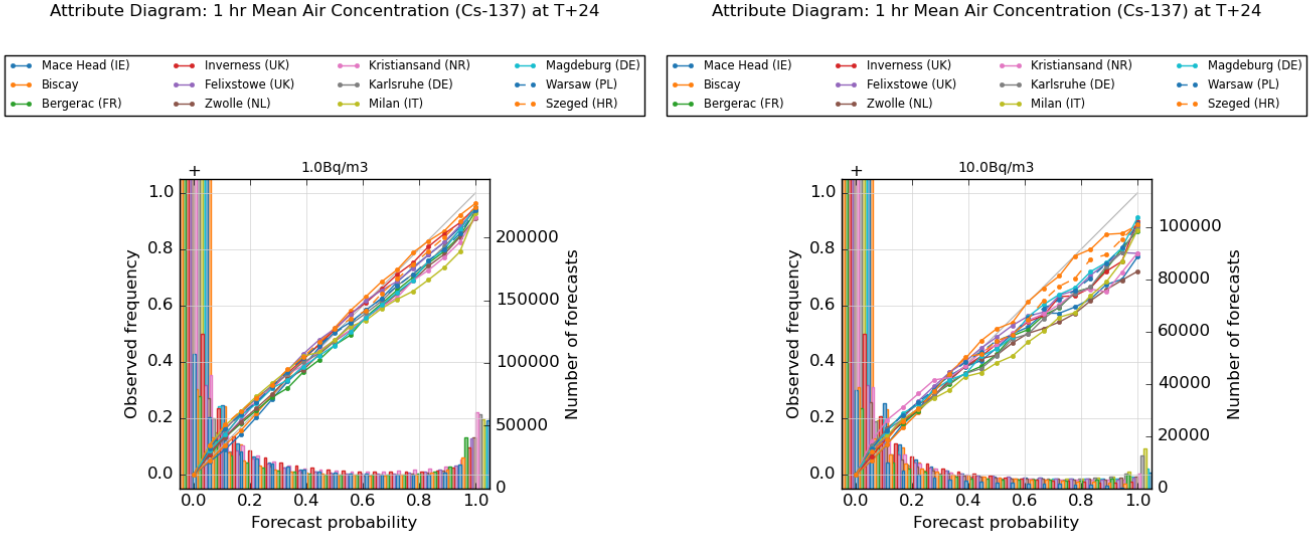

Figure S6. Attribute diagrams for exceedances of 1.0 Bq m^{-3} (left) and 10.0 Bq m^{-3} (right) for the 1-hour averaged air concentration after 24 hours, comparing the releases from each location.

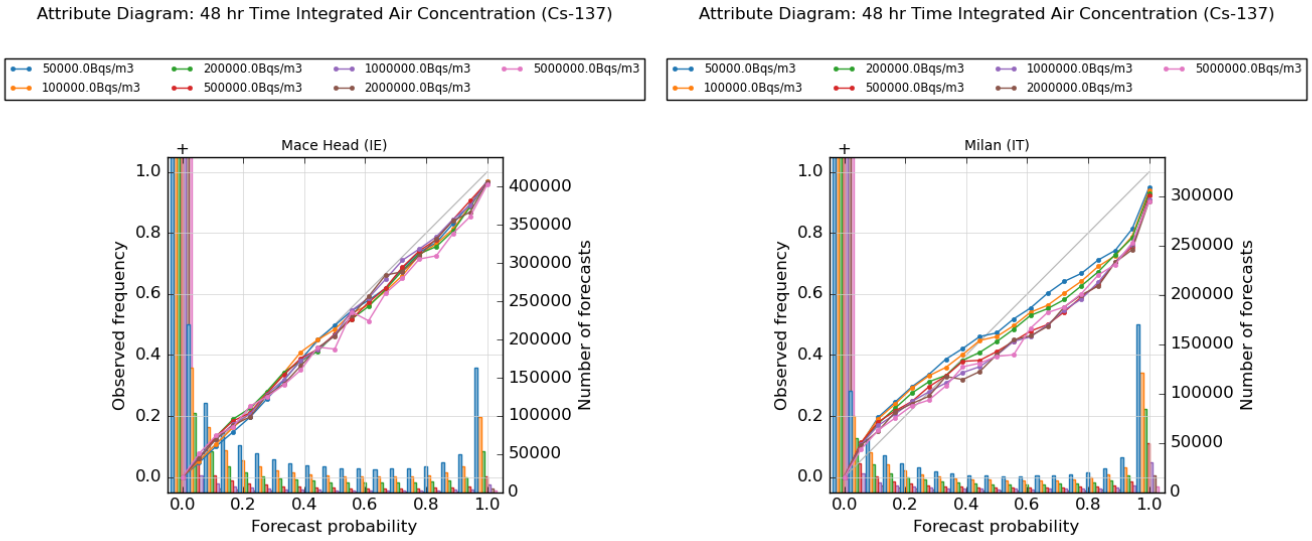

Figure S7. Attribute diagrams for 48-hour time-integrated air concentration at Mace Head (left) and Milan (right).

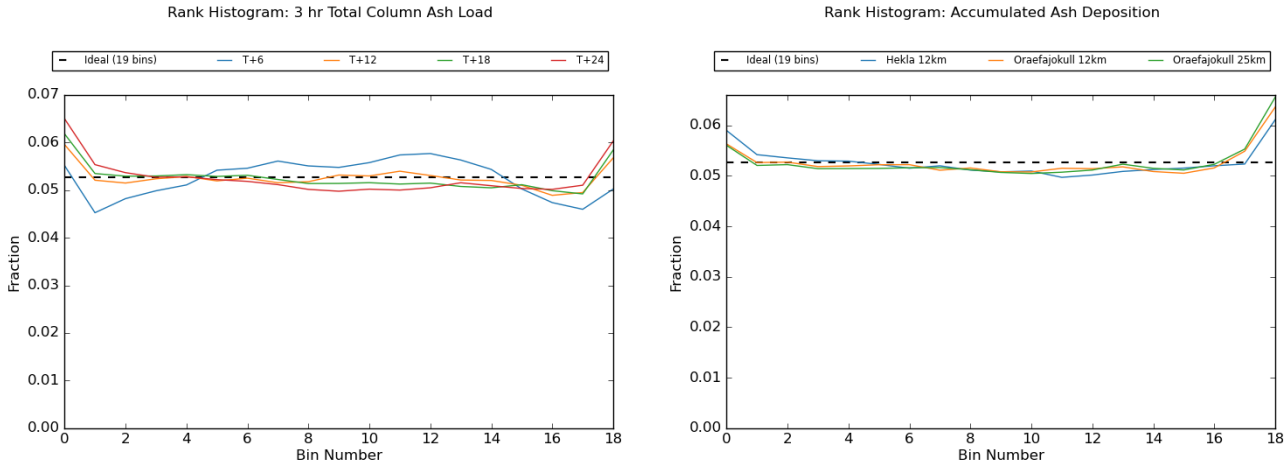

Figure S8. Rank histograms for 3-hour mean ash column load shown at 6 hour intervals (left) and the total deposited ash at T+24 (right). The ash column loads are based on the combined data from all three eruption scenarios, whereas the total deposited ash shows the three scenarios separately.

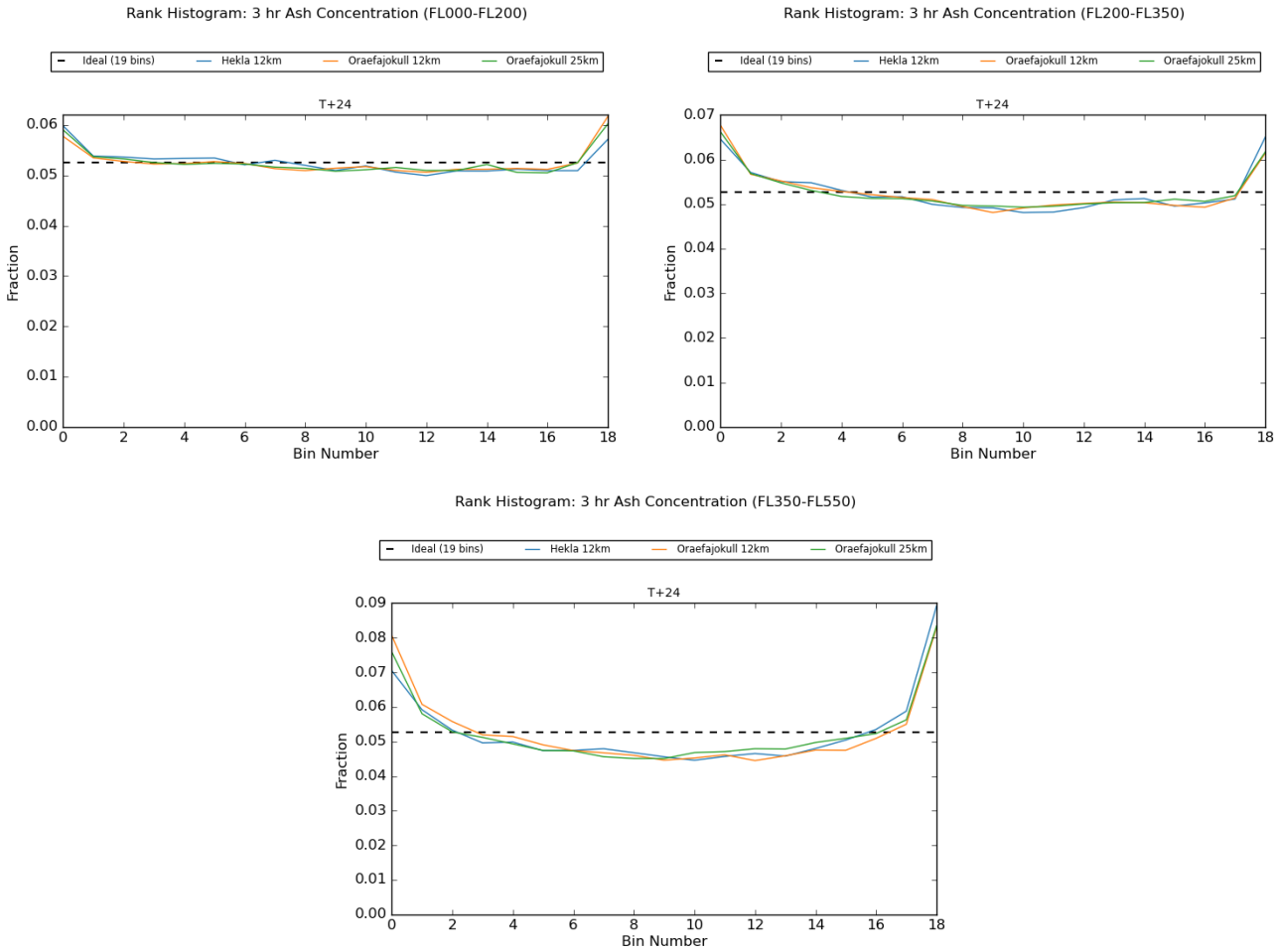

Figure S9. Rank histograms for 3-hour mean peak ash concentration at T+24 comparing between the three eruption scenarios. Plots show peak ash concentration in the three standard VAAC flight-level layers FL000-200 (top left), FL200-350 (top right) and FL350-550 (bottom).

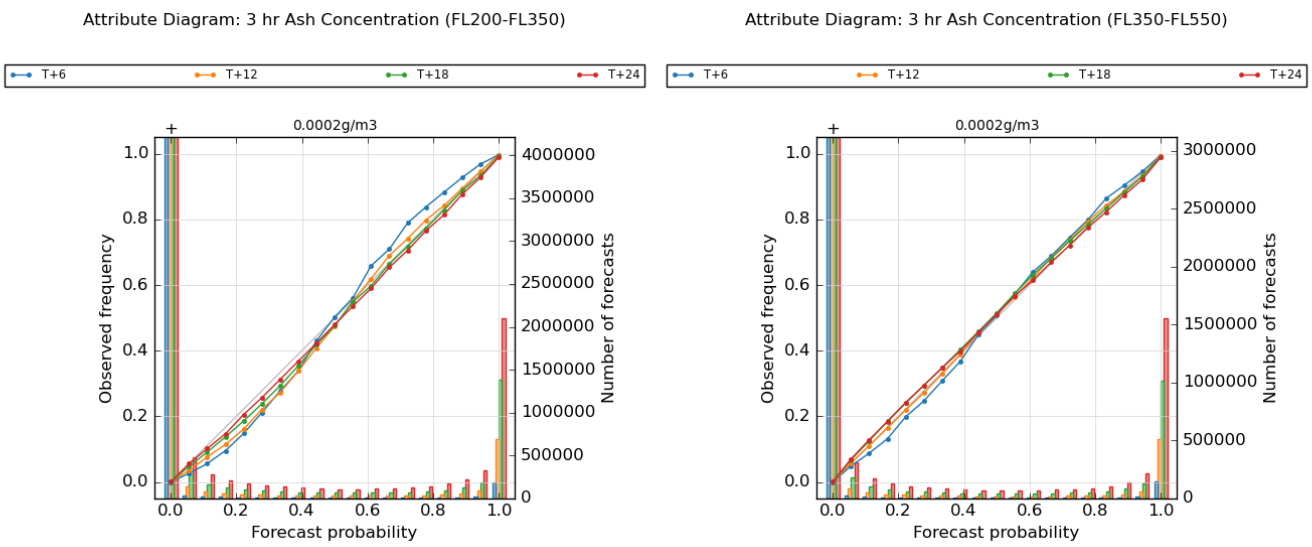

Figure S10. Attribute diagrams for 3-hour mean peak ash concentration in the middle flight-level layer FL200-350 (left) and upper layer FL350-550 (right) at 6 hour intervals from the start of the eruption to T+24. Plots are based on the combined data from all 3 eruption scenarios and are evaluated using an ash concentration threshold value of 0.2 mg m^{-3}.

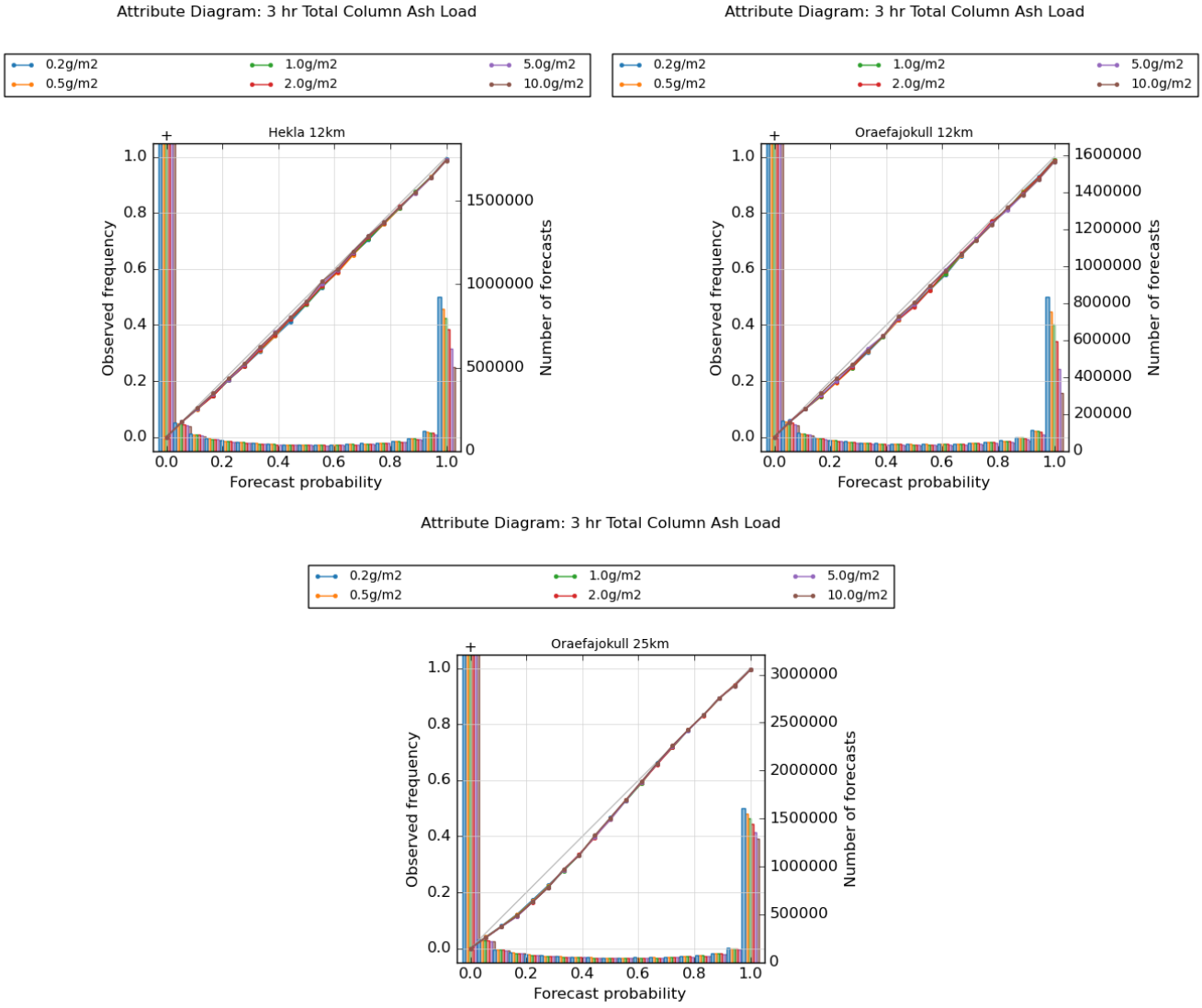

Figure S11. Attribute diagrams for 3-hour mean ash column load at T+24 for Hekla 12 km (top left), Öraefajökull 12 km (top right) and Öraefajökull 25 km (bottom).

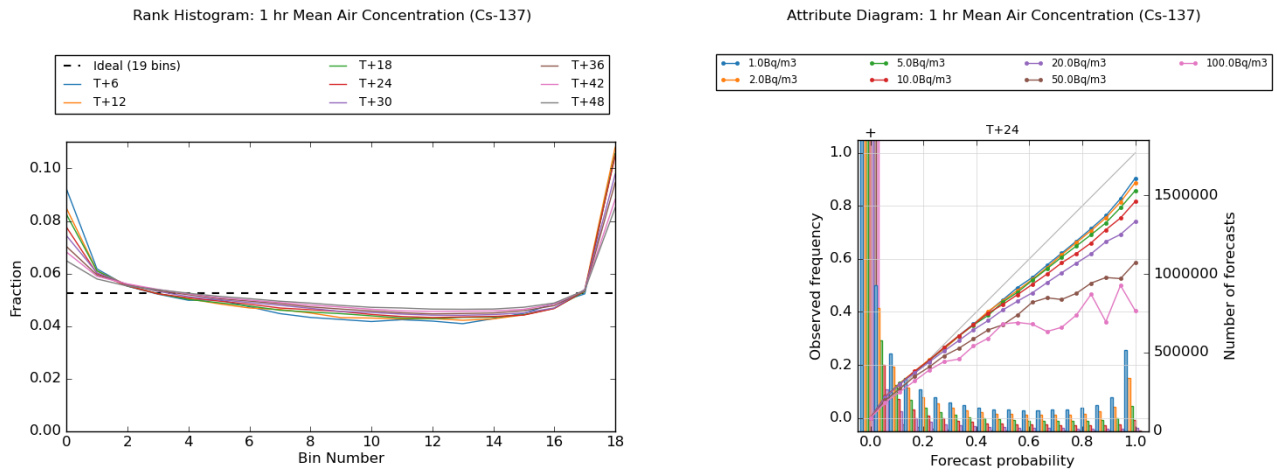

Figure S12. Rank histograms and attribute diagram for 1-hour mean air concentration in radiological case study when evaluated against ECMWF global analyses (c.f., Figures 2 and 6 in main paper).